Supporting information

Buckyball C_{60}/Fe-N_4 Superstructured Electrodes for Efficient Oxygen Reduction Reaction

Fancang Meng,[†,‡] Yinhui Zhang,[†,‡] Bohong Jiang,[†] Jiahao Li,[†] Huan Wu, [†] Jianwei Zhao, [††] Huihui Kong,[†,] Qingmin Ji [†,*]*

[†] Herbert Gleiter Institute for Nanoscience, School of Materials Science and Engineering, Nanjing University of Science & Technology, 200 Xiaolingwei, Nanjing, 210094, China

[††] Shenzhen Huasuan Technology Co., Ltd.

[‡] These authors contributed this work equally

* Corresponding author: jiqingmin@njust.edu.cn, konghuihui@njust.edu.cn

Additional experimental information

Characterizations. Scanning electron microscopy (SEM) was performed on FEI Quanta 250FEG field emission scanning electron microscope operating at 15 kV. Transmission electron microscopy (TEM) was operated on a Tecnai G220 at a voltage of 200 kV. Nitrogen sorption measurements were conducted on powder samples at 77K using an Autosorb-1 surface area and pore size analyzer (Gemini VII 2390). The specific surface areas were calculated based on the Brunauer Emmett Teller method (BET). X-ray diffraction (XRD) patterns were measured using a Bruker-AXS D8 Advance diffractometer. Raman spectra were recorded on a scattering Raman spectrometer (Renishaw-invia) using excitation radiation at 514 nm from an Ar^+ ion laser and under the power of 10 mW. Fourier transform infrared (FTIR) spectra were obtained by the FTIR spectrometer Nicolet S10 (Thermo Fisher).

DFT calculations. The spin-polarized density functional theories (DFT) were carried out by using the Vienna *Ab initio* Simulation Package (VASP).[s1] The DFT-D3 method is adopted to evaluate the van der Waals (vdW) interaction.[s4] The Perdew-Burke-Ernzerhof generalized-gradient approximation functional was used to describe the interaction between electrons.[s3] All-electron plane-wave basis sets with an energy cutoff of 400 eV. The vacuum region was set to be 15 Å to prevent the interaction

between two adjacent surfaces. The convergence threshold was set at 1×10^{-5} eV in total energy and 0.02 eV $Å^{-1}$ in force on each atom.

The reaction Gibbs free energy (ΔG) is defined as :

$$\Delta G = \Delta E + \Delta E_{ZPE} - T\Delta S \text{ (T=298.15K)},$$

in which ΔE, the reaction energy, ΔE_{ZPE}, zero-point energies, ΔS, the entropy difference from vibrational frequency calculations. The entropy of gas phase are obtained from the NIST database with standard condition.[s4]

References for supporting information

[s1] G. Kresse, J. Furthmüller, Efficiency of ab-initio total energy calculations for metals and semiconductors using a plane-wave basis set. Comput. Mater. Sci., 1996, 6, 15-50.

[s2] S. Grimme, Semiempirical GGA-type density functional constructed with a long-range dispersion correction. J. Comput. Chem. 2006, 27 (15), 1787–1799.

[s3] J. P. Perdew, K. Burke, M. Ernzerhof, Generalized Gradient Approximation Made Simple. Phys. Rev. L., 1996, 77(10), 3865-386.

[s4] Computational Chemistry Comparison and Benchmark Database. http://cccbdb.nist.gov/

Additional Data

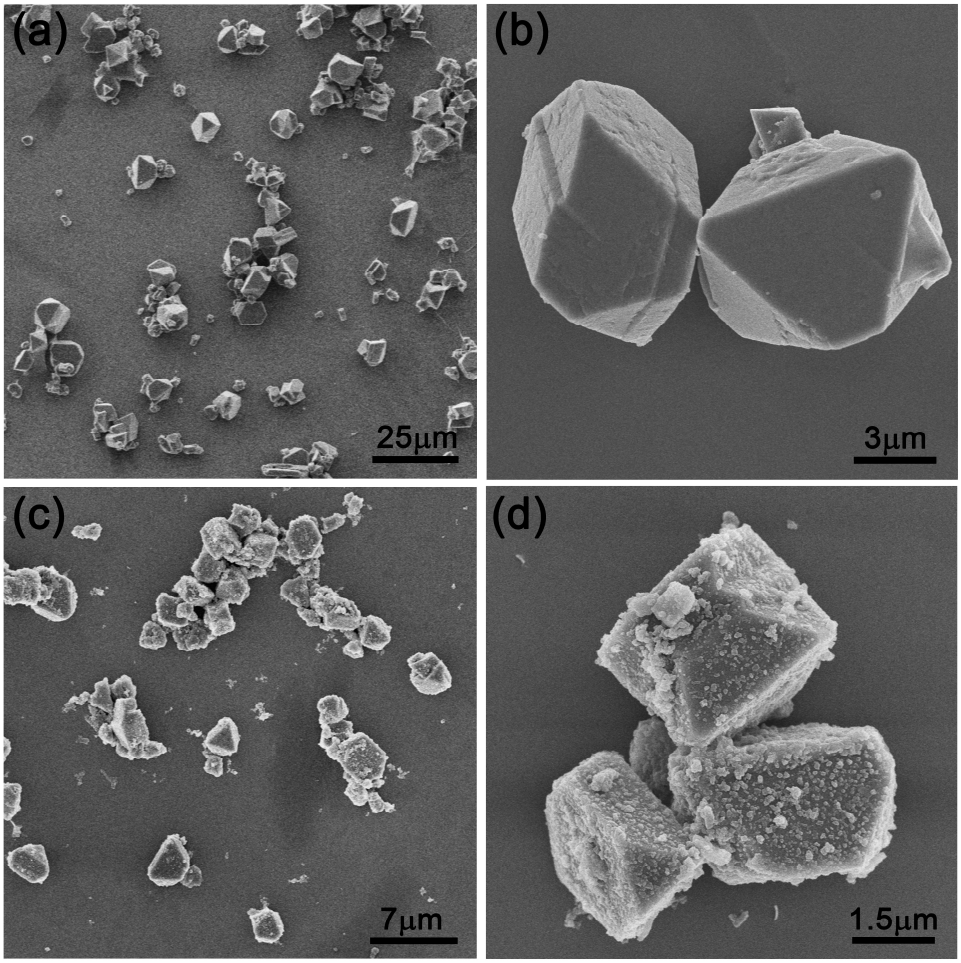

Figure S1. The SEM images of (a), (b) C_{60} particles by assembly in toluene/DMF mixture, and (c), (d) FePc-C_{60} particles by co-assembly in toluene/DMF mixture.

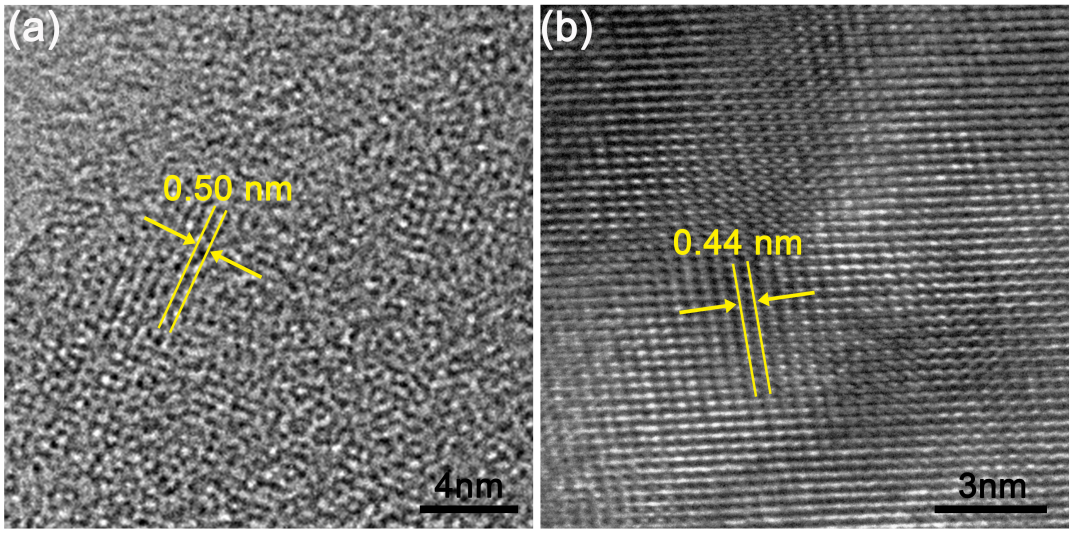

Figure S2. The HR-TEM images of (a) C_{60} particle and (b) FePc-C_{60} particles.

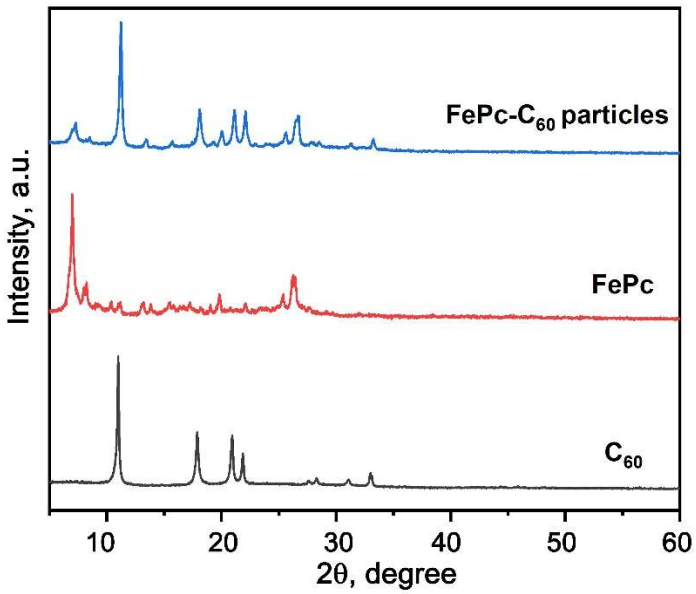

Figure S3. The XRD patterns of C_{60}, FePc and FePc-C_{60} particles.

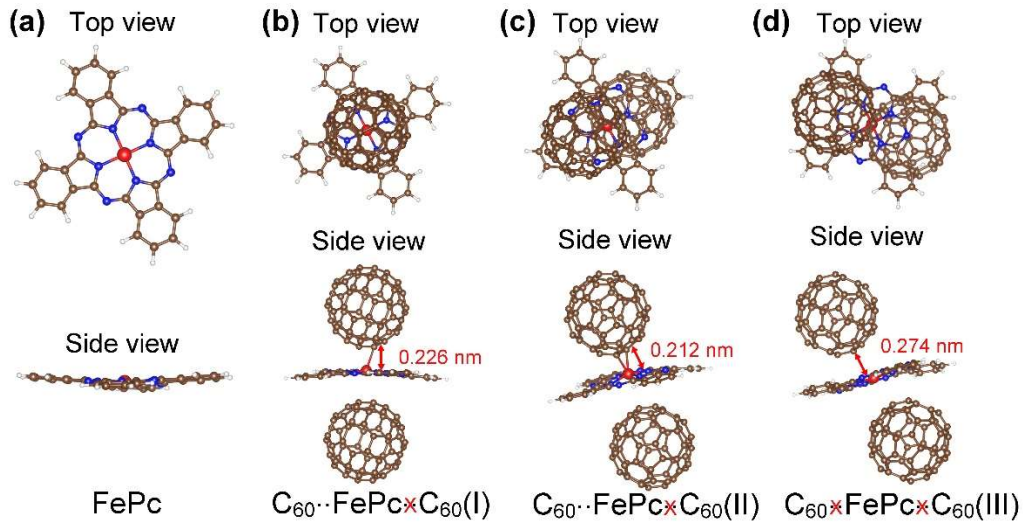

Figure S4. (a) The conformation of FePc and the complexation patterns for (b) the coordination of Fe in FePc (Fe@FePc) with pentagon carbon in C_{60} (C@C5-C_{60}), (c) the coordination of Fe@FePc with C-C@C5-C_{60} and (d) the coordination of N@FePc with C@C5-C_{60} with the optimal shortest distances based on DFT calculation. Atom color: brown, C; white, H; blue, N; red, Fe.

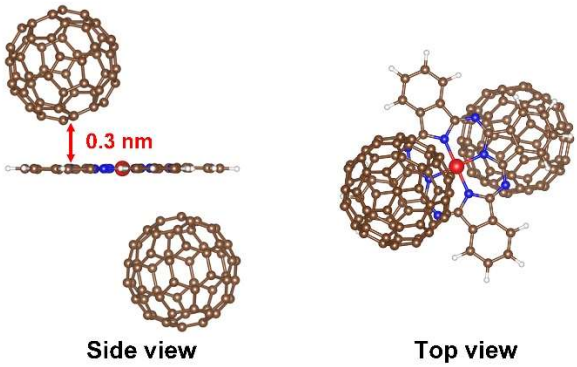

Figure S5. The complexation pattern by the coordination of C-C(pyrrole)@FePc with C-C@C5-C_{60} with the average shortest distances based on DFT calculation. Atom color: brown, C; white, H; blue, N; red, Fe.

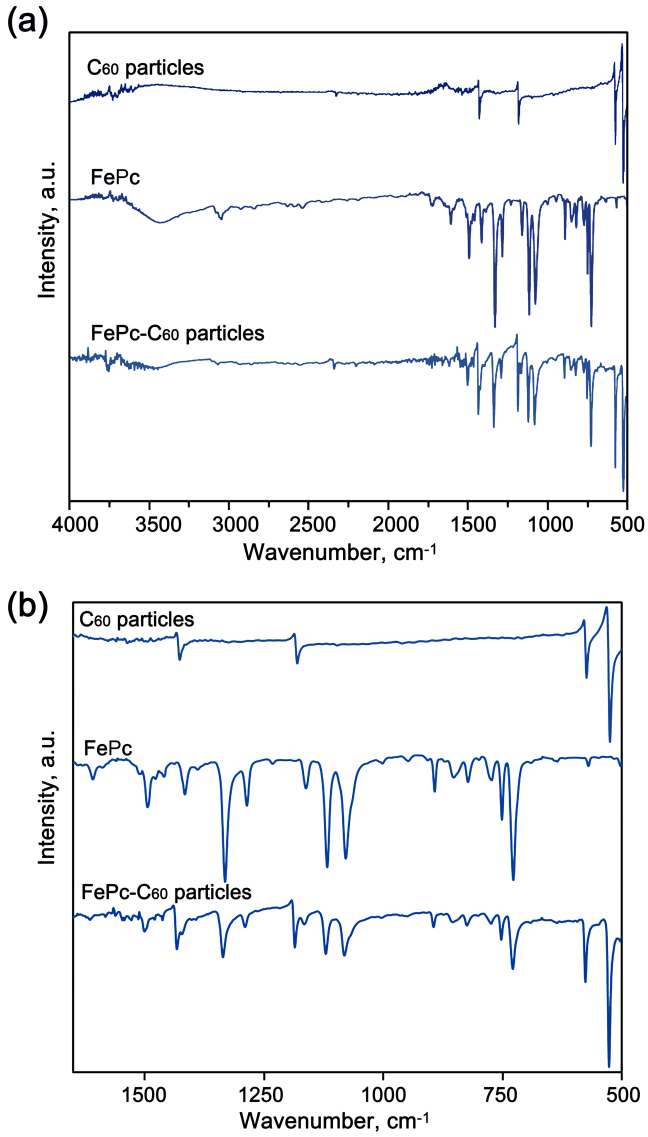

Figure S6. The FTIR spectra of C_{60} particle, FePc, and FePc-C_{60} particles.

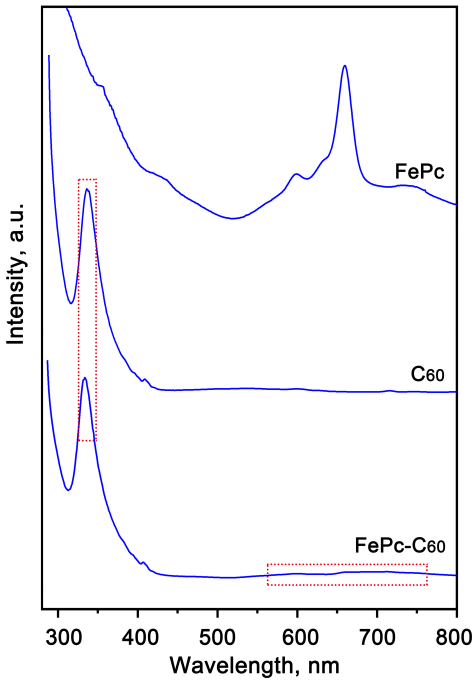

Figure S7. The UV-vis spectra of C_{60}, FePc, and FePc-C_{60}.

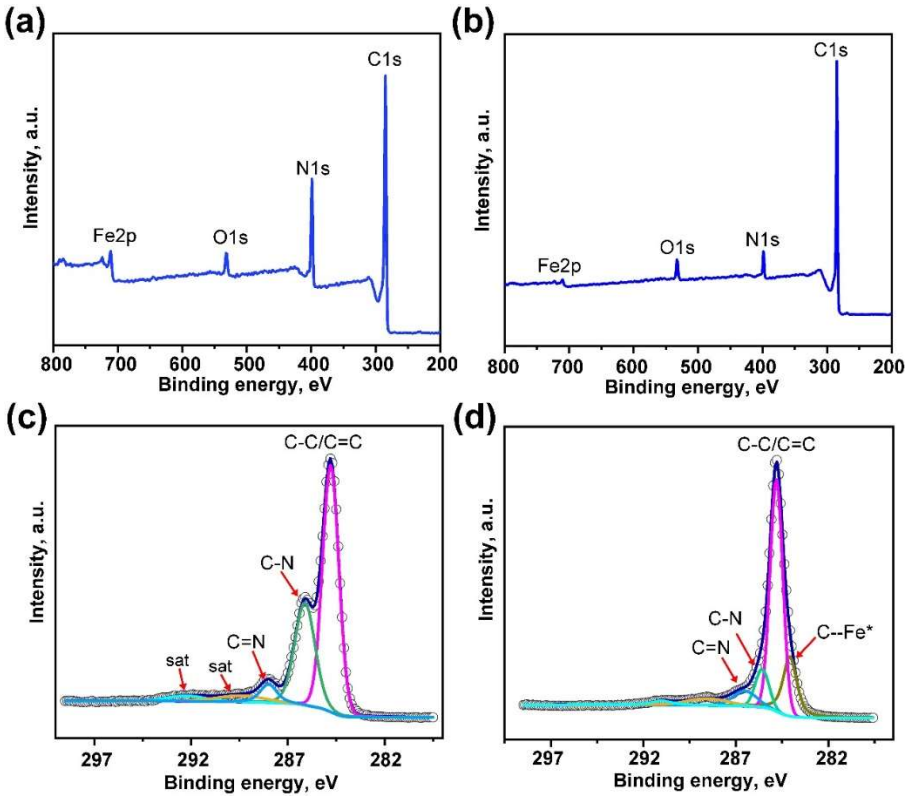

Figure S8. (a) The XPS spectrum and (c) C 1s spectrum of FePc. (b) The XPS spectrum and (d) C 1s spectrum of FePc-C_{60} particles.

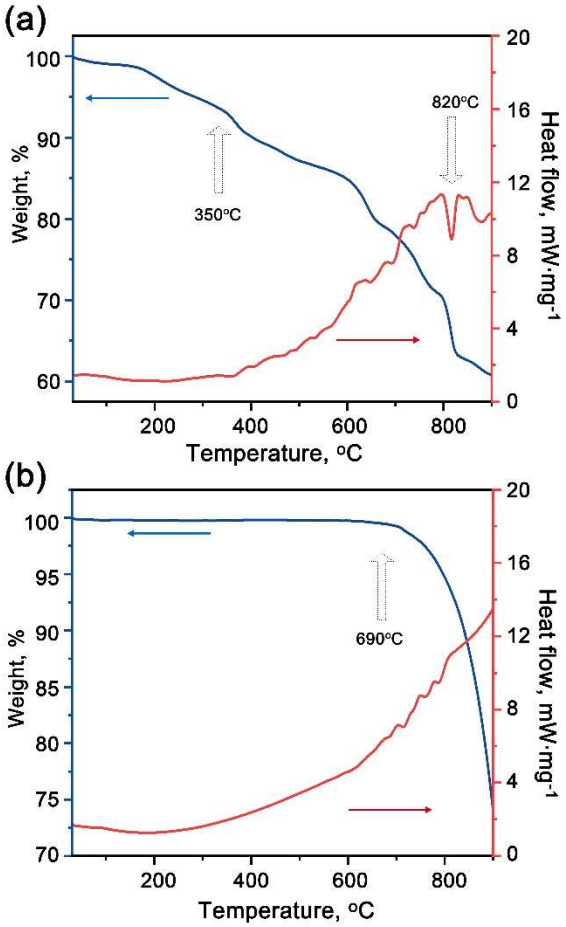

Figure S9. The TGA and DSC curves for (a) FePc, and (b) C_{60}.

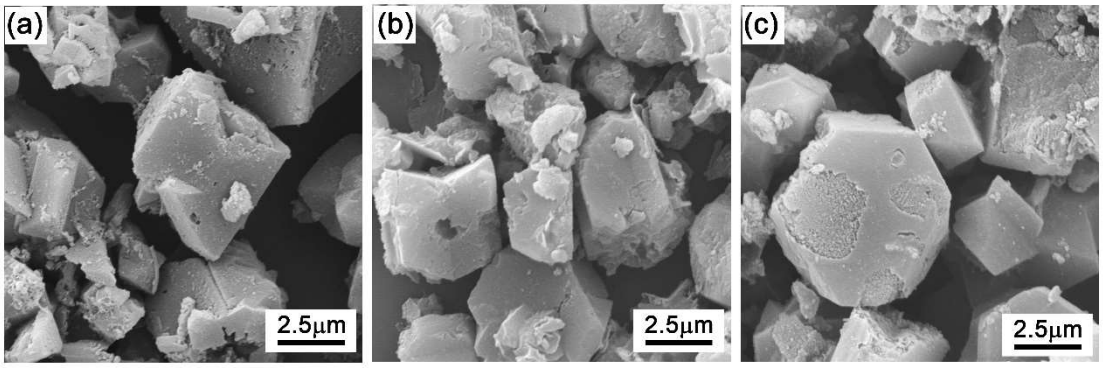

Figure S10. The SEM images of (a) FePc-C_{60}_500, (b) FePc-C_{60}_700 and (c) FePc-C_{60}_900.

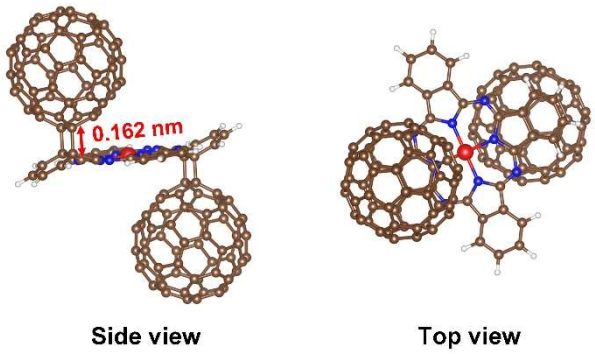

Figure S11. The convalent bonding based on the coordination pattern of C-C(pyrrole)@FePc with C-C@C5-C_{60} with the average shortest distances based on DFT calculation. Atom color: brown, C; white, H; blue, N; red, Fe.

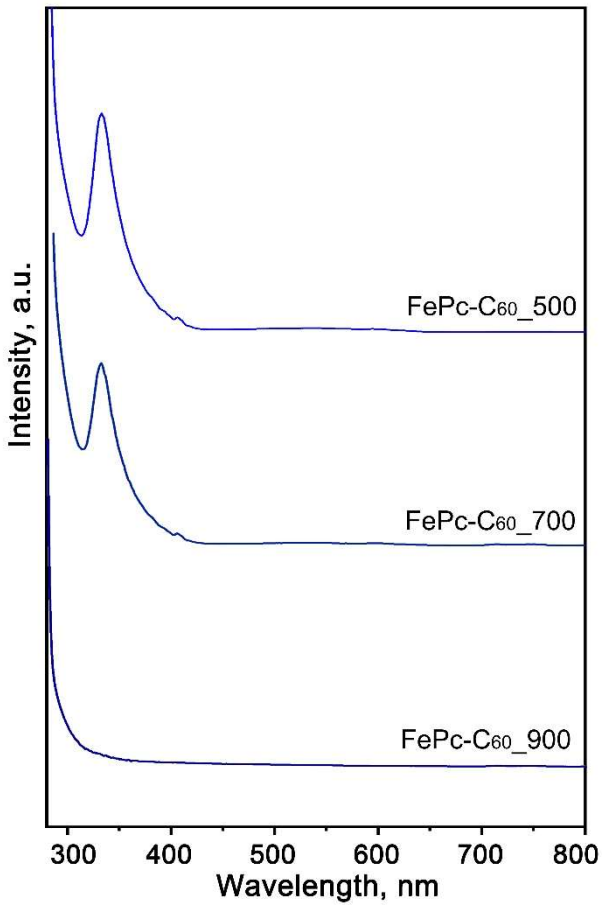

Figure S12. The UV-vis spectra of (a) FePc-C_{60}_500, (b) FePc-C_{60}_700, and (c) FePc-C_{60}_900.

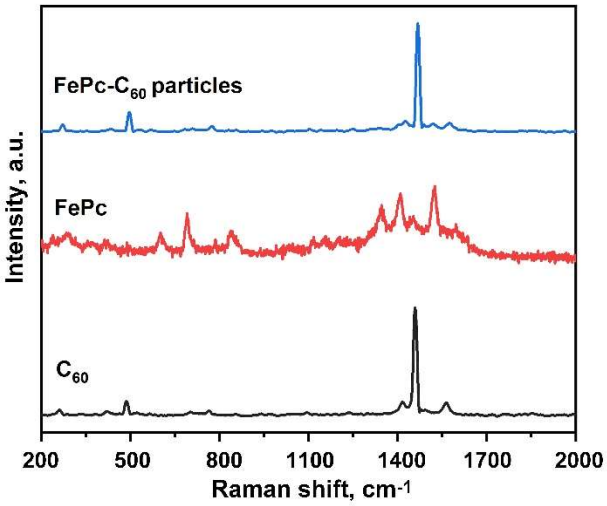

Figure S13. The Raman spectra of FePc-C_{60} particles, FePc, and C_{60}.

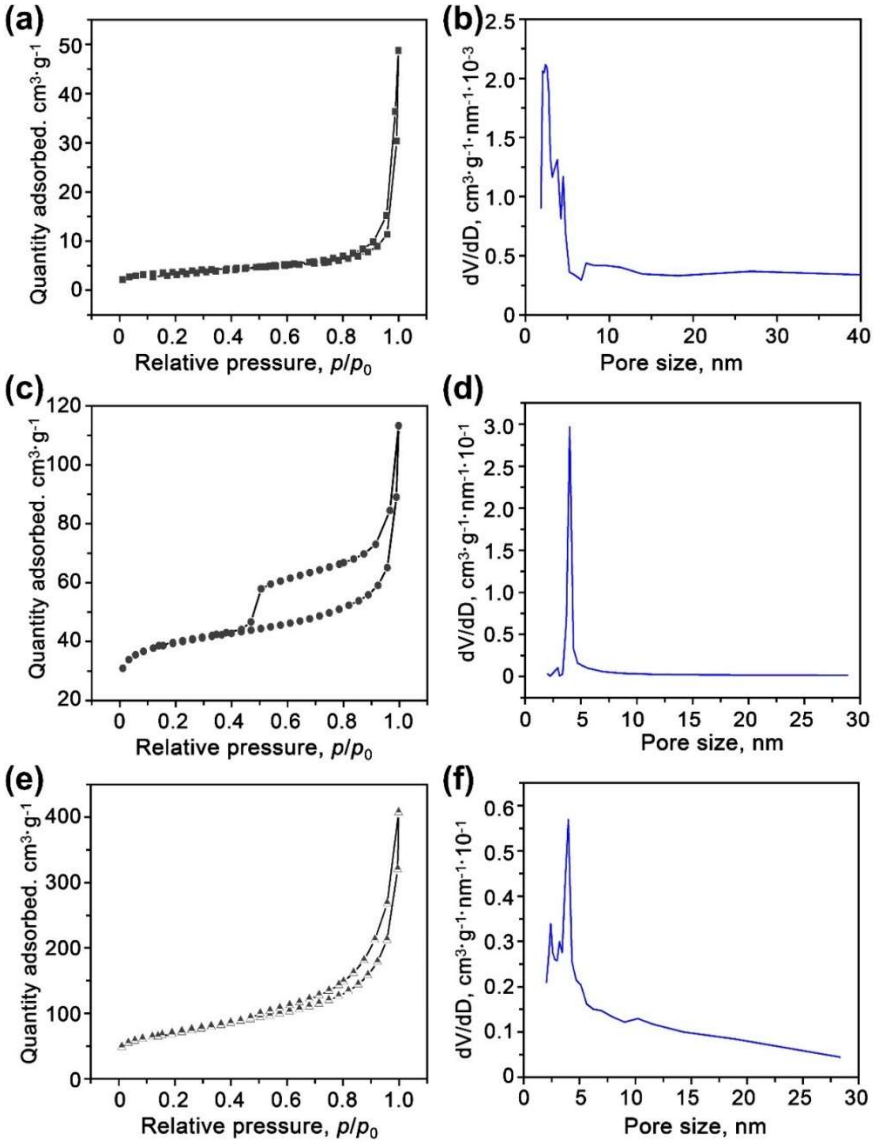

Figure S14. The N_2 isotherms of (a) FePc-C_{60}_500, (c) FePc-C_{60}_700, and (e) FePc-C_{60}_900. The pore size distribution of (b) FePc-C_{60}_500, (d) FePc-C_{60}_700, and (f) FePc-C_{60}_900.

Table S1. The porous characteristic properties of FePc-C_{60} carbon electrodes by nitrogen sorption measurements.

Sample	BET surface area ($m^2 \cdot g^{-1}$)	Average pore size (nm)	Pore volume ($cm^3 \cdot g^{-1}$)
FePc-C_{60}_500	12.68	21.28	0.075
FePc-C_{60}_700	125.00	10.32	0.175
FePc-C_{60}_900	239.31	9.33	0.329

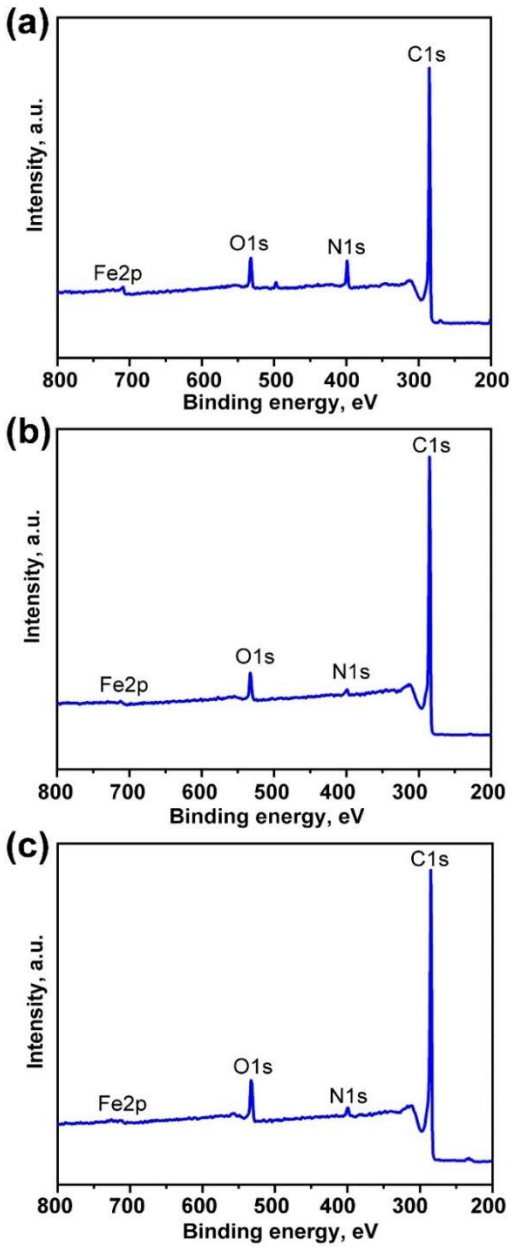

Figure S15. The XPS spectra of (a) FePc-C_{60}_500, (b) FePc-C_{60}_700, and (c) FePc-C_{60}_900.

Table S2. The calculated proportion of various elements states in FePc-C_{60} carbons based on the XPS analysis.

Samples	XPS		Based on N 1s spectra					Based on Fe 2p spectra
	N%	Fe%	Pyridinic N%	Pyrrolic N%	Graphite N%	Fe-N%	Fe_3N %	Fe^{2+}/Fe^{3+}
FePc	18.85	2.07	-	-	-	81.5[a]	-	1/0
FePc-C_{60}	6.70	0.80	-	-	-	75.8[a]	-	1/0
FePc-C_{60}_500	7.12	0.94	-	-	-	70.0[a]	-	1.35
FePc-C_{60}_700	2.28	0.39	12	24.9	14.2	33.8[b]	-	0.72
FePc-C_{60}_900	2.98	0.43	10.6	25.7	22.8	15.2[b]	3.3	0.55

a: be the form of Fe-N_4 (including pyrrolic N from FePc); b: be the forms of various Fe-N_x.

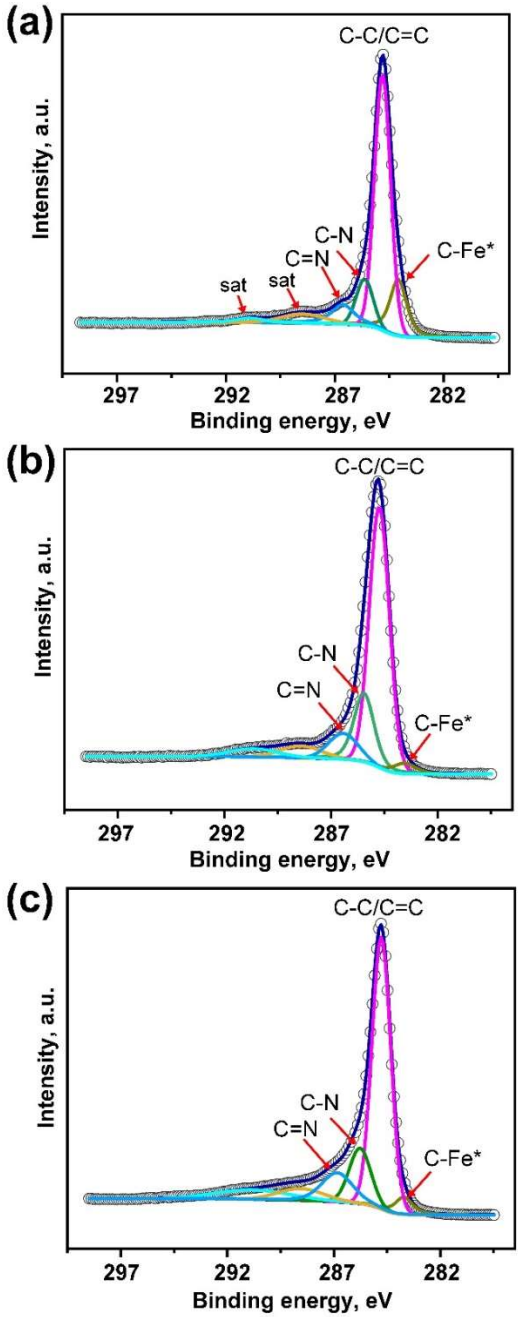

Figure S16. The XPS C 1s spectra of (a) FePc-C_{60}_500, (b) FePc-C_{60}_700, and (c) FePc-C_{60}_900.

.

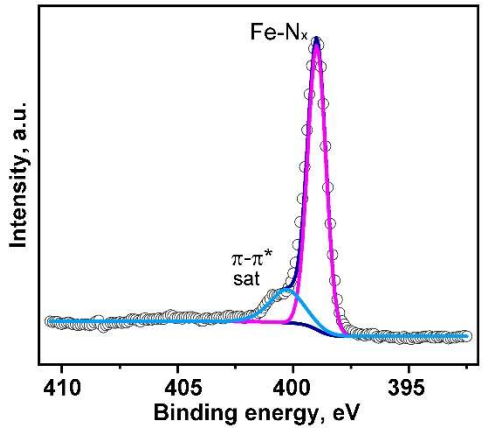

Figure S17. The XPS N 1s spectrum of FePc.

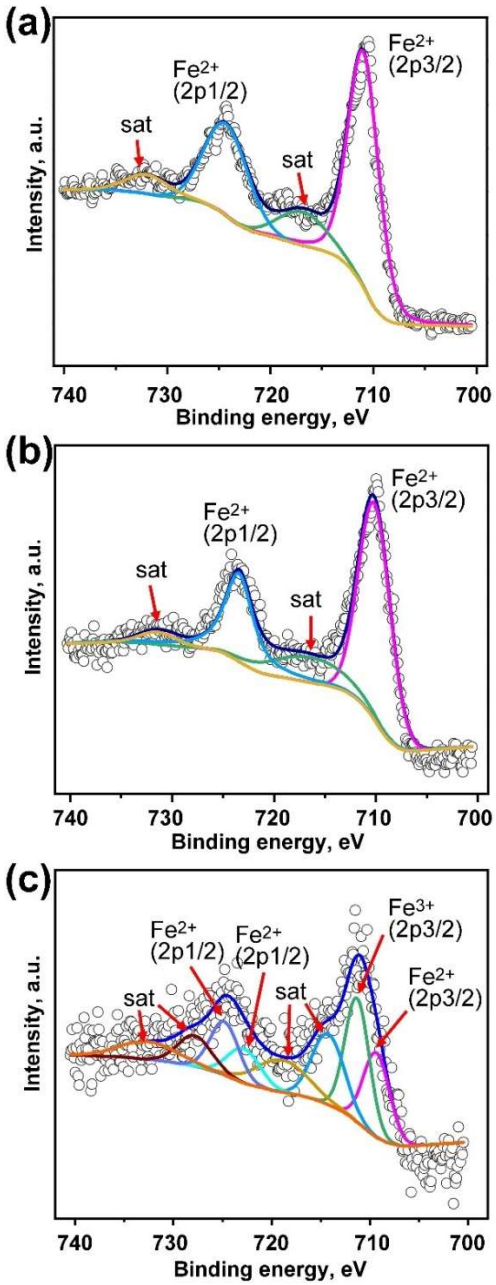

Figure S18. The Fe 2p XPS spectra (a) FePc, (b) FePc-C_{60}, and (c) FePc-C_{60}_700.

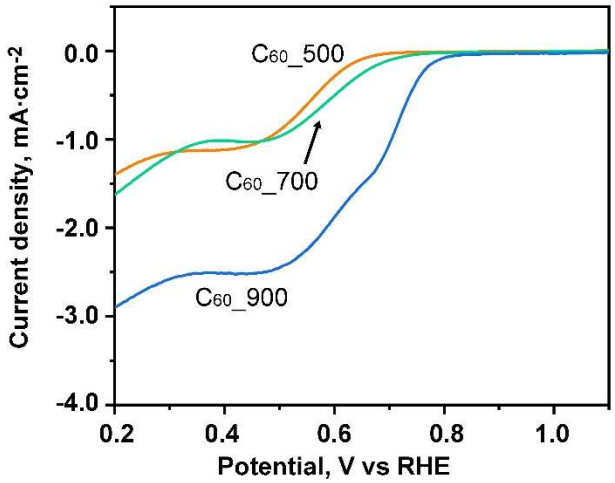

Figure S19. The LSV curves of C_{60}_500, C_{60}_700 and C_{60}_900.

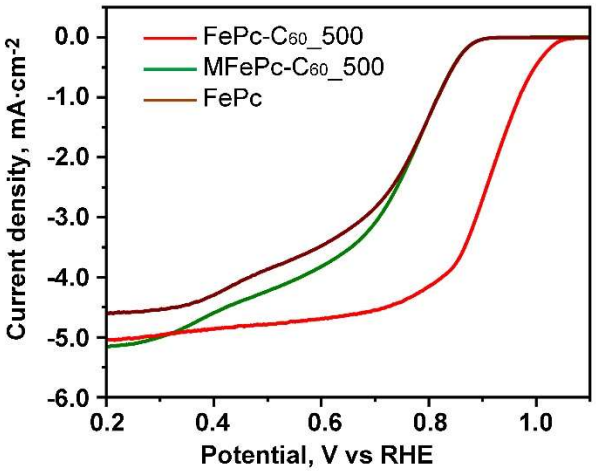

Figure S20. The LSV curves of FePc-C_{60}_500, FePc and MFePc-C_{60}_500.

Table S3. The comparison of ORR activities of FePc-C_{60} carbon electrodes, FePc, and Pt/C.

Sample	E_0 (V)	$E_{1/2}$ (V)	j_L(mA·cm^{-2})
FePc-C_{60}_500	1.04	0.91	5.05
FePc-C_{60}_700	0.92	0.73	4.27
FePc-C_{60}_900	0.97	0.84	4.53
MFePc-C_{60}_500	0.88	0.74	5.16
FePc	0.88	0.75	4.6
Pt/C	0.97	0.87	5.01

Table S4. The comparison of the ORR performance of the reported metal-doped C_{60}-derived electrocatalysts in alkaline medium.

Catalyst	E_0 (V)	$E_{1/2}$ (V)	j_L (mA·cm^{-2})	*Ref.*
FePc-C_{60}_500	1.04	0.91	5.05	**This work**
PD/N-C	0.911	0.833	5.29	1
MFC_{60}-130	0.82	0.76	-	2
FMN700	0.93	0.81	-	3
Fe-MFC_{60}-150	085	0.78	-	4
C_{60}@Co-N-PCM	0.98	0.85	5.5	5
Cu(15%)-MFC_{60}	0.86	0.76	5.18	6
N,S-PCNFs	0.969	0.837	5.50	7
N,S-PHCNSs-75	0.954	0.827	5.64	8
FNCNs-900	0.976	0.851	6.21	9
C_{60}/FeTPP-700	-	0.877	-	10
FeN/C_{60}O-900	0.98	0.85	5.23	11
FeN@FCS-900	0.93	0.78	4.2	12
CoTPP/C_{60}-800	0.93	0.824	5.5	13
FePc/FC	-	0.917	-	14
CNO-900	0.976	0.853	6.02	15
dFCMC	-	0.834	-	16

References for supporting information in Table S4

[s1] J. Zhu, Y. Huang, W. Mei, C. Zhao, C. Zhang, J. Zhang, I. S. Amiinu and S. Mu, *Angew. Chem. Int. Ed.*, 2019, **58**, 3859-3864.

[s2] M. R. Benzigar, S. Joseph, H. Ilbeygi, D.-H. Park, S. Sarkar, G. Chandra, S. Umapathy, S. Srinivasan, S. N. Talapaneni and A. Vinu, *Angew. Chem. Int. Ed.,* 2018, **57**, 569.

[s3] Z. Peng, Q. Jiang, P. Peng and F.-F. Li, *Eng. Sci.*, 2021, **14**, 27-38

[s4] M. R. Benzigar, S. Joseph, G. Saianand, A.-I. Gopalan, S. Sarkar, S. Srinivasan, D.-H. Park, S. Kim, S. N. Talapaneni, K. Ramadass and A. Vinu, *Microporous Mesoporous Mater.*, 2019, **285**, 21-31.

[s5] J. Wu, S. Wang, Z. Lei, R. Guan, M. Chen, P. Du, Y. Lu, R. Cao and S. Yang, *Nano Res.*, 2021, 14, 2596-2605.

[s6] G. Saianand, A. I. Gopalan, J. C. Lee, C. I. Sathish, K. Gopalakrishnan, G. E. Unni, D. Shanbhag, V. Dasireddy, J. Yi, S. Xi, A. H. Al-Muhtaseb and A. Vinu, *Small*, 2020, **16**, e1903937.

[s7] Z. He, P. Wei, N. Chen, J. Han and X. Lu, *Chem.-Eur. J.*, 2021, **27**, 1423-1429.

[s8] Z. He, P. Wei, T. Xu, J. Han, X. Gao and X. Lu, *Mater. Chem. Front.*, 2021, **5**, 7873-7882.

[s9] Z. He, Z. Zhou, P. Wei, T. Xu, J. Han, K. Huang, K. Guo, W. Huang, T. Akasaka, X. Lu, *Chem Asian J.*, 2023, **18**, e202200994.

[s10] H. Wang, L. Cao, Y. Feng, J. Chen,W. Feng, T. Luo, Y. Hu, C. Yuan, Y. Zhao, Y. Zhao, K. Kajiyoshi, Y. Liu, Z. Li and J. Huang, *Chin. Chem. Lett.*, 2023, **34**, 107601.

[s11] B. Jiang, S. Wang, F. Meng, L. Ju, W. Jiang, Q. Ji and H. D. Quan, *CrystEngComm*, 2022, **24**, 5783-5791.

[s12] L. Ju, G. Hao, F. Meng, W. Jiang and Q. Ji. *J. Mater. Chem. A*, 2023, **11**, 25534-25544.

[s13] A. Yu, Q. Huang, S. Gao, T. Xu, W. Zhang, N. Joshi, P. Peng, Y. Yang, F.-F. Li. *Carbon Future*, 2024, **1**, 9200009.

[s14] J. Chen, M. Wang, L. Chen, K. Guo, B. Liu, K. Wang, N. Li, L. Bao and X. Lu, *Adv. Energy Sustainability Res.*, 2024, **5**, 2400010

[s15] K. Guo, Z. He, S. Lu, P. Zhang, N. Li, L. Bao, Z. Yu, L. Song, X. Lu, *Adv. Funct. Mater.*, 2023, **33**, 2302100.

[s16] N. Li, M. Li, K. Guo, Z. Guo, R. Wang, L. Bao, G.L. Hou, X. Lu, *Adv. Energy Mater.*, 2024, **14**, 2401008.

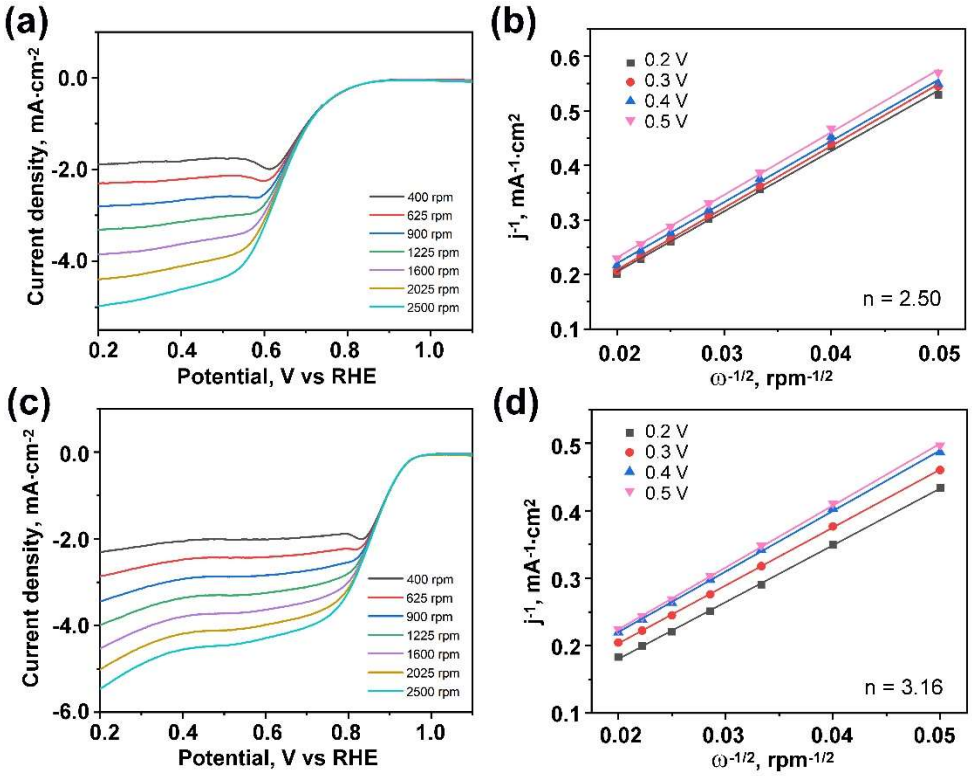

Figure S21. The LSV curves of (a) FePc-C_{60}_700 and (c) FePc-C_{60}_900 in O_2-saturated 0.1 M KOH solution at different rotating rates. The K-L plots of (c) FePc-C_{60}_700 and (d) FePc-C_{60}_900 at different potentials.

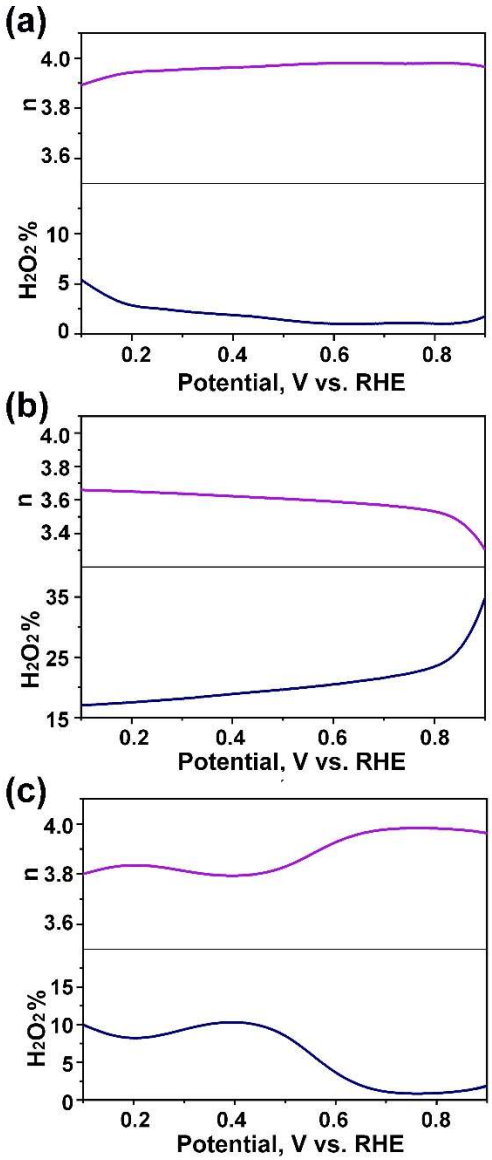

Figure S22. The electron transfer number (n) and H_2O_2% yield of (a) Pt/C, (b) FePc-C_{60}_700 and (c) FePc-C_{60}_900.

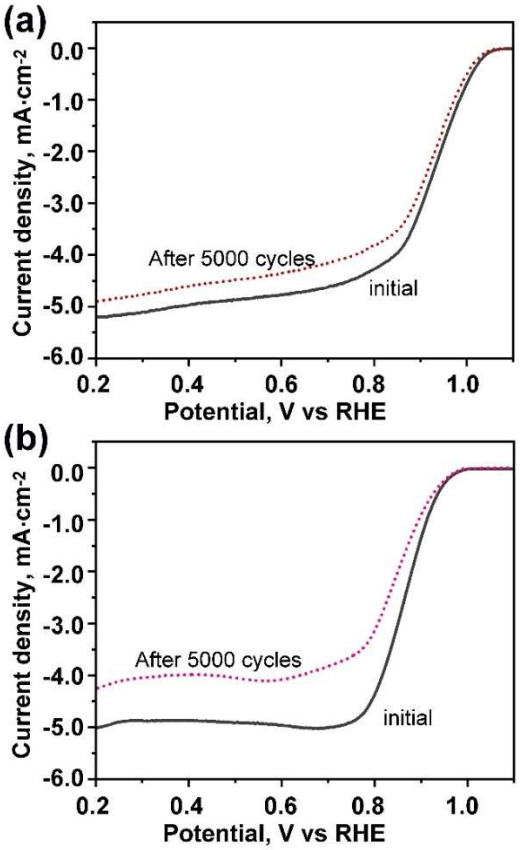

Figure S23. The LSV curves of (a) FePc-C_{60}_500 and (b) Pt/C in O_2-saturated 0.1 M KOH solution at 1600 rpm before and after 5000 potential cycles.

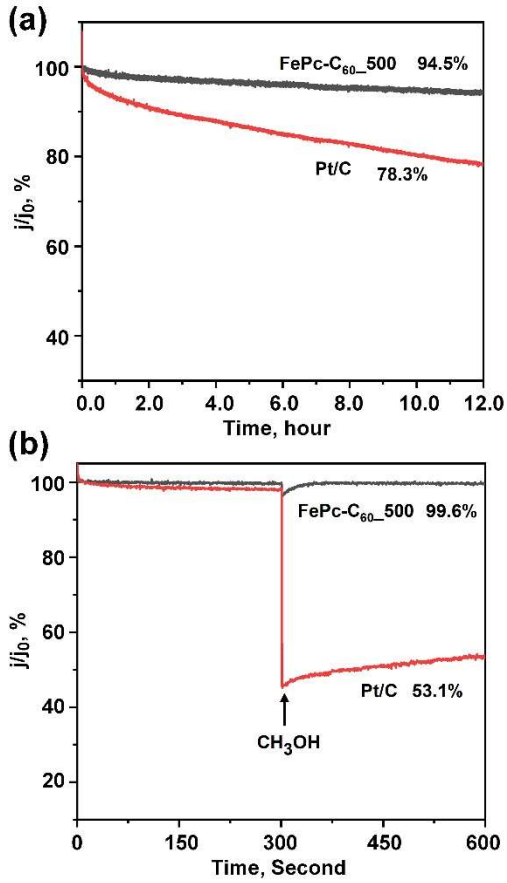

Figure S24. (a) The *i–t* response curves of FePc-C_{60}_500 and Pt/C. (b) The *i–t* response curves for the methanol immunity experiments of FePc-C_{60}_500 and Pt/C.